(Preprint) AAS 18-103

ATTITUDE CONTROL SYSTEM COMPLEXITY REDUCTION VIA TAILORED VISCOELASTIC DAMPING CO-DESIGN

Chendi Lin[*], Daniel R. Herber[†], Vedant[‡], Yong Hoon Lee[*], Alexander Ghosh[‡], Randy H. Ewoldt[*], James T. Alllison[†]

Intelligent structures utilize distributed actuation, such as piezoelectric strain actuators, to control flexible structure vibration and motion. A new type of intelligent structure has been introduced recently for precision spacecraft attitude control. It utilizes lead zirconate titanate (PZT) piezoelectric actuators bonded to solar arrays (SAs), and bends SAs to use inertial coupling for small-amplitude, high-precision attitude control and active damping. Integrated physical and control system design studies have been performed to investigate performance capabilities and to generate design insights for this new class of attitude control system. Both distributed- and lumped-parameter models have been developed for these design studies. While PZTs can operate at high frequency, relying on active damping alone to manage all vibration requires high-performance control hardware. In this article we investigate the potential value of introducing tailored distributed viscoelastic materials within SAs as a strategy to manage higher-frequency vibration passively, reducing spillover and complementing active control. A case study based on a pseudo-rigid body dynamic model (PRBDM) and linear viscoelasticity is presented. The tradeoffs between control system complexity, passive damping behavior, and overall dynamic performance are quantified.

INTRODUCTION

High-precision attitude control is crucial for space data gathering. To obtain high quality scientific data, fast and accurate small angle reorientation and jitter reduction are needed.[1–4] Many studies have been performed to diminish the vibration by both structural and control design.[5–7] Recent work has suggested that strain-actuated solar arrays (SASAs) have potential to effectively achieve this goal by using distributed internal actuation across the SAs.[2] This internal actuation can be achieved with piezoelectric actuators bonded to the SAs.[8] While this control architecture performs well, additional tailoring of the structure may increase the overall performance as well reduce system complexity and cost.

As a case study, viscoelastic dampers are introduced at the joints between the SAs and the main spacecraft body. Using a simplified model of the system, we can investigate how intelligent structures can effectively achieve enhanced attitude control on the spacecraft. In addition to designing aspects of the SA geometry, we will consider some design flexibility with respect to the properties of the viscoelastic material. Previous studies have investigated the design of the linear viscoelastic

---

[*] Mechanical Science and Engineering, University of Illinois at Urbana-Champaign, 1206 W. Green St., Urbana, IL 61801

[†] Industrial and Enterprise Systems Engineering, University of Illinois at Urbana-Champaign, 104 S. Mathews Ave., Urbana, IL 61801

[‡] Aerospace Engineering, University of Illinois at Urbana-Champaign, 104 S. Wright St., Urbana, IL 61801

material function (a function-valued material property) using simple parameterizations to improve system performance.[9] Other studies have shown that the simultaneous design of physical structure and material properties enables higher system performance compared to designing structure only.[10] Here we use a general relaxation kernel function with Boltzmann superposition to represent linear viscoelasticity.[11,12] This model gives the most general representation of linear viscoelastic behavior, which can be characterized by the relaxation kernel function $K(t)$ and integro-differential equations. In this article, we choose some specific kernel function shapes. Using these kernel functions, we will investigate the capability of the viscoelastic material damper to generate improved designs that can maximize the reorientation capabilities of the bus and minimize vibrations.

MODELING OF THE SPACECRAFT BUS, STRAIN-ACTUATED SOLAR ARRAYS, AND VISCOELASTIC ELEMENTS

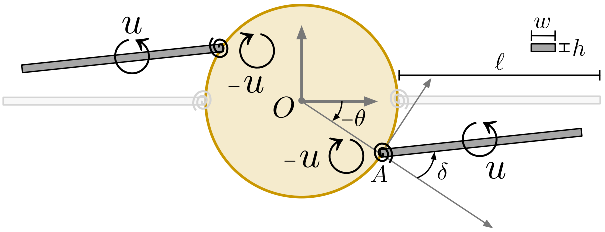

Figure 1. Pseudo-rigid body dynamic model of the SASA system.

Pseudo-Rigid Body Dynamic Model

An illustration of the SASA system is in Fig. 1. Here the spacecraft bus is modeled as a simple cylinder attached to two flexible SASAs. In this system, actuation is only provided through strain at the SA structure surface created by applying voltage on the attached piezoelectric actuators and there is no interaction with anything external to the spacecraft. Then, the total system momentum must be conserved (in the absence of any external disturbances). Therefore, for a generally counterclockwise (CCW) movement of the SA, the bus will rotate in the opposing clockwise (CW) direction allowing for attitude changes.

The key behavior of the SASA system can be captured by a fairly simple pseudo-rigid body dynamic model (PRBDM),[2,13] shown in Fig. 1. Two rigid cantilever beams representing the SAs are linked to the bus cylinder via a torsional spring. The stiffness of the SAs beams is modeled with the torsional springs. The rotation angle of the spacecraft bus about its center O is denoted θ, δ denotes the rotation angle of the SA around the joint A (and is an approximation of the strain on the SA), and M is the moment applied on the array via the piezoelectric actuator. The geometry of the SA is defined by ℓ as the length, w as the width, and h as the height.

Equations of Motion for PRBDM SASA System. It was shown by Chilan et al. that the expected array bending displacement is small.[2] Therefore, a linearized bus-array PRBDM is appropriate. The linearized equations are:

$$\mathcal{M}\begin{bmatrix}\ddot{\theta}\\ \ddot{\delta}\end{bmatrix}+\mathcal{B}\begin{bmatrix}\dot{\theta}\\ \dot{\delta}\end{bmatrix}+\mathcal{K}\begin{bmatrix}\theta\\ \delta\end{bmatrix}=\mathcal{T} \tag{1a}$$

$$\text{where: } \mathcal{M}=\begin{bmatrix}m_{11} & m_{12}\\ m_{21} & m_{22}\end{bmatrix}, \quad \mathcal{B}=\begin{bmatrix}0 & 0\\ 0 & b_{22}\end{bmatrix}, \quad \mathcal{K}=\begin{bmatrix}0 & 0\\ 0 & 2k\end{bmatrix}, \quad \mathcal{T}=\begin{bmatrix}0\\ 2\end{bmatrix}u+\begin{bmatrix}q\\ 0\end{bmatrix} \tag{1b}$$

$$m_{11} = J_\theta + 2J_\delta + \frac{1}{2}m\ell^2 + 2m\ell r + 2mr^2 \tag{1c}$$

$$m_{12} = m_{21} = 2J_\delta + \frac{1}{2}m\ell^2 + m\ell r, \quad m_{22} = 2J_\delta + \frac{1}{2}m\ell^2 \tag{1d}$$

$$m = \rho\ell wh, \quad J_\delta = \frac{1}{12}m\left(\ell^2 + h^2\right) \tag{1e}$$

where k is the SA stiffness, b_{22} will help us include the viscoelastic element, the two factors in $\mathcal{T}$ and $\mathcal{K}$ are due to the two symmetrically attached SAs, and q is the potential disturbance on the bus. By inverting the mass matrix and rearranging, we arrive at the equivalent first-order linear dynamic system:

$$\dot{\boldsymbol{\xi}}_r = \boldsymbol{A}_r\boldsymbol{\xi}_r + \boldsymbol{B}_r u + \boldsymbol{d}_r \tag{2a}$$

$$\frac{d}{dt}\begin{bmatrix}\theta\\ \dot{\theta}\\ \delta\\ \dot{\delta}\end{bmatrix} = \begin{bmatrix}0 & 1 & 0 & 0\\ 0 & 0 & 2\Delta m_{12}k & \Delta m_{12}b_{22}\\ 0 & 0 & 0 & 1\\ 0 & 0 & -2\Delta m_{11}k & -\Delta m_{11}b_{22}\end{bmatrix}\begin{bmatrix}\theta\\ \dot{\theta}\\ \delta\\ \dot{\delta}\end{bmatrix} + \begin{bmatrix}0\\ -2\Delta m_{12}\\ 0\\ 2\Delta m_{11}\end{bmatrix}u + \begin{bmatrix}0\\ \Delta m_{22}q\\ 0\\ -\Delta m_{21}q\end{bmatrix} \tag{2b}$$

where $\Delta^{-1} = (m_{11}m_{22} - m_{12}m_{21})$.

We also in this section, want to link the beam stiffness k to the SA geometry for a more realizable physical system. Using beam theory on a cantilever beam, we have the following relationship between the strain and the applied moment:

$$u = k\delta = \frac{2EIv}{\ell^2} \tag{3}$$

where u is the moment applied on the beam, E is the Young's modulus, v is the deflection of the beam at the tip, and $I = wh^3/12$ is the moment of inertia of the beam's cross section. Using again the small-angle approximation, we have:

$$\delta \approx \sin\delta = \frac{v}{\ell} \tag{4}$$

Thus the relationship between k and ℓ, both with and without an area constraint, is:

$$k = \frac{Ewh^3}{6\ell} \text{ or } k = \frac{A_0Eh^3}{6\ell^2} \text{ when } A_0 = w\ell \tag{5}$$

Modeling the Viscoelastic Element

Here we consider the addition of a viscoelastic damper at the revolute joint that attaches the SA to the spacecraft bus. The viscoelasticity in the damper in this study is characterized by the relaxation kernel function $K(t)$. Theoretically, the shape of the kernel function of the linear viscoelasticity in time domain may have any arbitrary shape, but with a certain constraints: larger or equal to zero and monotonically decreasing (see the viscoelastic damper design test cases in Refs. 12, 14). Here we aim to enhance system performance by optimizing the shape of this function using an efficient parameterization. The torque (or force) induced by the relative motion of the joint (both δ and $\dot{\delta}$) containing a viscoelastic damper is modeled with the following equation:

$$F_{VE}(t) = F_k(t) + F_{CI}(t) = -k_s\delta(t) - \int_{-\infty}^{t} K(t-\tau)\dot{\delta}(\tau)d\tau \tag{6}$$

where F_{VE} is the torque due to a viscoelastic element, F_k is the torque due to the spring behavior parameterized by k_s, and F_{CI} is the torque due to the convolution integral behavior parameterized by the relaxation kernel $K(t)$.

Simulation and optimization studies that require the evaluation of a convolution integral can be computationally expensive.[15,16] Fortunately, there are alternative representations that can reduce the computational expense, such as an linear time-invariant (LTI) system representations.

Representation as an LTI System. Consider the following single-input, single-output LTI system:

$$\dot{\boldsymbol{\xi}}_s(t) = \boldsymbol{A}_s \boldsymbol{\xi}_s(t) + \boldsymbol{B}_s u_s(t) \tag{7a}$$

$$y_s(t) = \boldsymbol{C}_s \boldsymbol{\xi}_s(t) \tag{7b}$$

where $\boldsymbol{\xi}_s$ are the states and the matrices $\{\boldsymbol{A}_s, \boldsymbol{B}_s, \boldsymbol{C}_s\}$ are of the appropriate size. The solution to Eqn. (7) without $\boldsymbol{\xi}_s(t)$ can be represented as :[17]

$$y_s(t) = \boldsymbol{C}_s e^{\boldsymbol{A}_s(t-t_0)} \boldsymbol{\xi}_s(t_0) + \int_{t_0}^{t} \boldsymbol{C}_s e^{\boldsymbol{A}_s(t-\tau)} \boldsymbol{B}_s u_s(\tau) d\tau \tag{8}$$

We can now show an equivalence between Eqns. (6) and (8) with:

$$\dot{\delta}(t) \Leftrightarrow u_s(t), \quad F_{CI}(t) \Leftrightarrow y_s(t), \quad K(t-\tau) \Leftrightarrow -\boldsymbol{C}_s e^{\boldsymbol{A}_s(t-\tau)} \boldsymbol{B}_s \tag{9}$$

with the assumption that all forces due to the damper at and before t_0 are negligible (i.e., $\boldsymbol{\xi}_s(t_0) = \boldsymbol{0}$ and the lower limit of integration in Eqn. (6) can be replaced with t_0).[17] However, these representations are only equivalent if there exists a set of LTI matrices that exactly represent $K(t)$. Otherwise, Eqn. (8) is only an approximation of Eqn. (6), but for many forms of $K(t)$, a reasonably low-order system can provide a sufficient approximation.[17] This approximation is used in other domains such as the integral in Cummins' equation for heaving bodies in waves used to compute the radiation force.[18]

The key advantage of the LTI system approximation is that the system of integro-differential equations is converted into a system of ordinary differential equations.[17]Therefore, standard simulation and dynamic optimization techniques can be readily applied. Furthermore, this approximation adds additional linear dynamics. If the original dynamic model, excluding the convolution integral, was linear, then the dynamic model with remain linear with this approximation. Therefore, linear systems theory as well as other techniques suitable for linear systems can be readily applied.

Realization of the LTI System. One method for realizing the required state-space form is to directly minimize the error between the $K(\tau)$ and $\boldsymbol{C}_s e^{\boldsymbol{A}_s \tau} \boldsymbol{B}_s$:

$$\min_{\boldsymbol{A}_s, \boldsymbol{B}_s, \boldsymbol{C}_s} \quad \left\| K(\tau) - \boldsymbol{C}_s e^{\boldsymbol{A}_s \tau} \boldsymbol{B}_s \right\|_2^2 \tag{10}$$

where we would need to choose the number of additional states n_s. Since we cannot evaluate the error at all values of τ, we can define a grid of points, denoted $\boldsymbol{t}$, in the regions of interest and evaluate the error at those points only. Typically, a large value of n_s results in a better approximation, but the system size increases, which can lead to increase computational expense when evaluating the linear system. Unfortunately, directly tuning the entries in the matrices requires a large number of optimization variables (exactly $n_s^2 + 2n_s$). Alternatively, as suggested in Ref. 17, we can utilized the companion-form realization:

$$\boldsymbol{A}_s = \begin{bmatrix} 0 & 0 & 0 & \cdots & 0 & -a_1 \\ 1 & 0 & 0 & \cdots & 0 & -a_2 \\ 0 & 1 & 0 & \cdots & 0 & -a_3 \\ 0 & 0 & 1 & \cdots & 0 & -a_4 \\ \vdots & \vdots & \vdots & \ddots & \vdots & \vdots \\ 0 & 0 & 0 & \cdots & 1 & -a_n \end{bmatrix}, \quad \boldsymbol{B}_s = \begin{bmatrix} b_1 \\ b_2 \\ b_3 \\ b_4 \\ \vdots \\ b_n \end{bmatrix}, \quad \boldsymbol{C}_s = \begin{bmatrix} 0 & 0 & 0 & \cdots & 0 & 1 \end{bmatrix} \tag{11}$$

where we now only need to determine $2n_s$ unknown parameters, denoted $\boldsymbol{a}$ and $\boldsymbol{b}$.

We can further reduce the number of parameters noting that $\boldsymbol{a}$ and $\boldsymbol{b}$ are the coefficients of the numerator and denominator in the transfer function representation of the linear system. Therefore, we can instead perform the fitting process with respect to the poles $\boldsymbol{p}$ and zeros $\boldsymbol{z}$ directly. This reduces the number of parameters to $2(n_s - 1)$, but has the additional advantage that we can place limits on the magnitude of poles. The poles are eigenvalues of the state transition matrix $\boldsymbol{A}_s$, and it can be advantageous to keep them within a certain range for numerical reasons.

The final reduction in the number of parameters is based on that for given values of $\boldsymbol{p}$, the values of $\boldsymbol{z}$ can be found with a least square estimate from the resulting overdetermined linear system (assuming the number of points in $\boldsymbol{t}$ is greater than or equal to n_s). Then the final suggestion nonlinear fitting problem is:

$$\min_{\boldsymbol{p}} \quad \left\| [\boldsymbol{X}] \left([\boldsymbol{X}]^{\mathsf{T}} [\boldsymbol{X}] \right)^{-1} [\boldsymbol{X}]^{\mathsf{T}} [K]_{\tau=\boldsymbol{t}} \right\|_2^2 \tag{12a}$$

$$\text{subject to:} \quad \boldsymbol{p}_{\min} \le \boldsymbol{p} \le \boldsymbol{p}_{\max} \tag{12b}$$

$$\text{where:} \quad [\boldsymbol{X}] = \left[\boldsymbol{C}_s e^{\boldsymbol{A}_s(\boldsymbol{p})\tau} \right]_{\tau=\boldsymbol{t}} \tag{12c}$$

where $[\cdot]_{\tau=\boldsymbol{t}}$ denotes the resulting matrix evaluated on $\boldsymbol{t}$. We now have only have $n_s - 1$ poles that need to be placed. We also note that poles may be real valued or come in complex-conjugate pairs; this is another decision that must be made during the fitting process. Since this a potentially highly nonlinear problem, global optimization techniques, in conjunction with gradient-based optimization, should be utilized to improve the likelihood of finding a suitable approximation. Finally, since the companion form is not ideal for simulation (typically results in large state values), the modal form is used instead.

Both the efficiency and robustness of this approach are important if we seek to handle more complex relaxation kernels or directly design the kernel function shape. For instance, the approximation would need to be updated for every change in the kernel function. Further investigation into methods of realizing this approximation more robustly and efficiently remains future work. However, we can explore different variations of the kernel on the single kernel function form using scaling.

Scaling the Kernel Function. Consider the following scaled kernel function $\bar{K}$:

$$K(\tau) = K_s \bar{K}(t_s \tau), \qquad K_s, t_s > 0 \tag{13}$$

where K_s is the amplitude scale and t_s is the time scale. We can apply this transformation to the output equation:

$$\begin{aligned}\int_{-\infty}^{t} K(t-\tau)\dot{\delta}(\tau)d\tau &= \int_{-\infty}^{t} K_s\bar{K}(t_s(t-\tau))\dot{\delta}(\tau)d\tau \\ &= \lim_{t_0\to-\infty}\left(K_s\bar{\boldsymbol{C}}_s e^{\bar{\boldsymbol{A}}_s t_s(t-t_0)}\boldsymbol{\xi}_s(t_0) + \int_{t_0}^{t} K_s\bar{\boldsymbol{C}}_s e^{\bar{\boldsymbol{A}}_s t_s(t-\tau)}\bar{\boldsymbol{B}}_s\dot{\delta}(\tau)d\tau\right) \\ &= \lim_{t_0\to-\infty}\left(\boldsymbol{C}_s e^{\boldsymbol{A}_s(t-t_0)}\boldsymbol{\xi}_s(t_0) + \int_{t_0}^{t} \boldsymbol{C}_s e^{\boldsymbol{A}_s(t-\tau)}\boldsymbol{B}_s\dot{\delta}(\tau)d\tau\right) \qquad (14)\end{aligned}$$

where $\boldsymbol{A}_s = t_s\bar{\boldsymbol{A}}_s$, $\boldsymbol{B}_s = \bar{\boldsymbol{B}}_s$, and $\boldsymbol{C}_s = K_s\bar{\boldsymbol{C}}_s$. Therefore, we can obtain a scaled state-space model from a related kernel function.

Combined Model

Here, we combine the models of the SASA system with the viscoelastic element. The damping force $b_{22}\dot{\delta}$ in Eqn. (2) is replaced by the LTI system in Eqn. (7) representing the viscoelastic element. The complete linear state-space including the scaling parameters for $\bar{K}$ is:

$$\dot{\boldsymbol{\xi}} = \boldsymbol{A}\boldsymbol{\xi} + \boldsymbol{B}u + \boldsymbol{d} \qquad (15a)$$

$$\frac{d}{dt}\begin{bmatrix}\theta \\ \dot{\theta} \\ \delta \\ \dot{\delta} \\ \boldsymbol{\xi}_s\end{bmatrix} = \begin{bmatrix}0 & 1 & 0 & 0 & \boldsymbol{0} \\ 0 & 0 & 2\Delta m_{12}k & 0 & \Delta m_{12}K_s\bar{\boldsymbol{C}}_s \\ 0 & 0 & 0 & 1 & \boldsymbol{0} \\ 0 & 0 & -2\Delta m_{11}k & 0 & -\Delta m_{11}K_s\bar{\boldsymbol{C}}_s \\ \boldsymbol{0} & \boldsymbol{0} & \boldsymbol{0} & \bar{\boldsymbol{B}}_{\boldsymbol{s}} & t_s\bar{\boldsymbol{A}}_s\end{bmatrix}\begin{bmatrix}\boldsymbol{\xi}_r \\ \boldsymbol{\xi}_s\end{bmatrix} + \begin{bmatrix}\boldsymbol{B}_r \\ \boldsymbol{0}\end{bmatrix}u + \begin{bmatrix}\boldsymbol{d}_r \\ \boldsymbol{0}\end{bmatrix} \qquad (15b)$$

With the modeling section complete, we can discuss the different design problem formulations.

DESIGN PROBLEM FORMULATION

Maximum Slew Amount

The goal of the first design problem is to investigate if the viscoelastic element can improve the maximum amount of rotation, or slew, the bus can achieve while still being able to hold the bus steady. Previous studies have shown fundamental limits on the slew magnitude as a consequence of the momentum conservation property of the system as well as additional constraints in the system.[2,13]

Multi-Phase Co-Design Problem Formulation. This design problem is formulated as a multi-phase dynamic optimization problem. The two phases are 1) a slewing phase where the spacecraft bus is rotated from some orientation to the origin, and 2) a holding phase where the bus is held close stationary about the origin. The time horizon between 0 and t_f is split into the two phases by t_m, or the time to perform the slew maneuver. This design problem is also a combined plant and control, or co-design, problem due to the design variables including the physical aspects of the system as

Table 1. Co-design problem parameters.

Parameter	Value	Parameter	Value
$u_{\max}$	20 N·m	A_0	3 m^2
$\epsilon_{\max}$	10^{-3}	V_0	0.054 m^3
$\ell_{\min}$	0.5 m	E	1.57 GPa
$\ell_{\max}$	2.5 m	J_θ	372.49 kg·m^2
θ_h	10^{-12} rad		
ϑ_h	10^{-12} rad/s		

well as the SA control moment.[2] The complete simultaneous co-design optimization problem is:

$$\min_{u,\ell,t_s,K_s} \quad -\theta(0) \tag{16a}$$

$$\text{subject to:} \quad \dot{\boldsymbol{\xi}} = \boldsymbol{A}(\ell, t_s, K_s)\boldsymbol{\xi} + \boldsymbol{B}(\ell)u + \boldsymbol{d}(\ell) \qquad \text{all phases} \tag{16b}$$

$$|u(t)| \leq u_{\max} \tag{16c}$$

$$|\epsilon| = \left|\frac{\delta(t)}{\ell}\right| \leq \epsilon_{\max} \tag{16d}$$

$$0 \leq t_s, K_s \tag{16e}$$

$$\ell_{\min} \leq \ell \leq \ell_{\max} \tag{16f}$$

$$\dot{\theta}(0) = \dot{\delta}(0) = 0, \ \delta(0) = 0, \ \boldsymbol{\xi}_s(0) = \mathbf{0} \qquad \text{phase 1 only (slew)} \tag{16g}$$

$$\theta(t) \leq \theta_h, \ \dot{\theta}(t) \leq \dot{\theta}_h \qquad \text{phase 2 only (hold)} \tag{16h}$$

where Eqn. (16a) represents the objective of maximum the slew amount of the bus, Eqn. (16b) enforces the linear dynamics described in the previous section, Eqn. (16c) is a limit on the maximum allowable control moment, Eqn. (16d) is a limit on the maximum allowable strain in the SA, Eqn. (16e) enforces nonnegativity of the scaling parameters for the viscoelastic element, and Eqn. (16f) bounds the SA length between a minimum and maximum value. The phase 1 specific constraints are in Eqn. (16g) and represent zero initial conditions for all the states except the bus angle. The phase 2 specific constraints are in Eqn. (16h) and represent the holding of the bus stationary about some small tolerances denoted by θ_h and ϑ_h. We also include both a volume and planform area constraint on the SAs to meet the same mission power and weight requirements. Therefore, the width and height of the SAs are defined by ℓ, the specified area A_0, and specified volume V_0. Many problem elements are based on the similar problem formulations used by Chilan et al.[2] and Herber and Allison.[13] The parameters selected in this study are shown in Table 1.

Scaled Optimization Problem. To achieve higher accuracy and better computational efficiency, the original optimization problem was scaled according to simple linear scaling relationships.[13] The time continuum, original states $\boldsymbol{\xi}_r$, and control are all scaled. The control was scaled using $u = u_{\max}\bar{u}$, while the time continuum with $t = t_m\bar{t}$. The states were scaled using the following matrix:

$$\boldsymbol{\xi} = \boldsymbol{T}\bar{\boldsymbol{\xi}}, \quad \text{where: } \boldsymbol{T} = \mathrm{diag}\left(\theta_{\text{nom}}, \frac{\theta_{\text{nom}}}{t_m}, \epsilon_{\max}\ell, \frac{\epsilon_{\max}\ell}{t_m}, \boldsymbol{I}\right) \tag{17}$$

where diag constructs a block diagonal matrix and $\theta_{\text{nom}} = 10^{-3}$ (selected based on the expected approximate magnitude of the slew maneuvers).

Solution Method. For fixed values of the plant variables $\boldsymbol{x}_p = [\ell, t_s, K_s]$, u is the only remaining optimization variable. Consequently, Prob. (16) is a linear-quadratic optimization (LQDO) problem. LQDO problems can be solved efficiently using direct transcription and quadratic programming.[19,20] Therefore, a nested co-design optimization approach is adopted.[21] The outer loop optimizes the plant variables with respect to the plant-only constraints, while for every candidate plant variable vector, the inner-loop LQDO problem is solved.

Disturbance-to-Output Reduction

The second problem aims to investigate the value of viscoelastic damper in reducing vibrations induced by disturbances with different frequencies. Intelligent structure has been shown to be effective in damping out vibrations.[22] In this study, the vibration magnitudes are compared between the case without damper, and the cases with viscoelastic damper involved. The amplitude scale and the time scale are varied to observe the trend of the disturbance-to-output reduction. The parameters are the same as what are shown in Table 1. Instead of performing full optimization for K_s and t_s, only several cases are presented to bring insights to future design. The magnitudes of vibrations of both the bus rotation θ and the solar array bending δ will be discussed.

RESULTS

Comparison with Simple SASA Problem

To validate that the code works correctly, the dimensionless quantities $\Pi = \frac{kt_f^2}{4\pi^2 J}$ from this study without damper and from simple SASA problem[2,13] are compared, where k is the stiffness of the solar arrays, t_f is the end time of the slewing phase, J is a constant relating the inertia of bus and the solar arrays. Π is supposed to be a constant with different t_f posed in the problem.

With the end time of the slewing phase varied, Π basically stays the same in the no-damper case. Column ”ratio” in Table 2 shows the comparison of Π in simple SASA problem and that in this study. The ratios are close to 1, which validate the formulation and the code. The small difference should be attributed to the fact that the simple problem does not link the stiffness and inertia ratio.

Table 2. Comparison of constant Π in simple SASA problem to Π in this study without viscoelastic damper. Good agreements are shown, validating the code.

	t_f	Π	ratio
Simple SASA	–	0.0866	–
Without Viscoelastic Damper	0.02	0.0843	1.0272
Without Viscoelastic Damper	0.2	0.0842	1.0281
Without Viscoelastic Damper	2	0.0842	1.0281

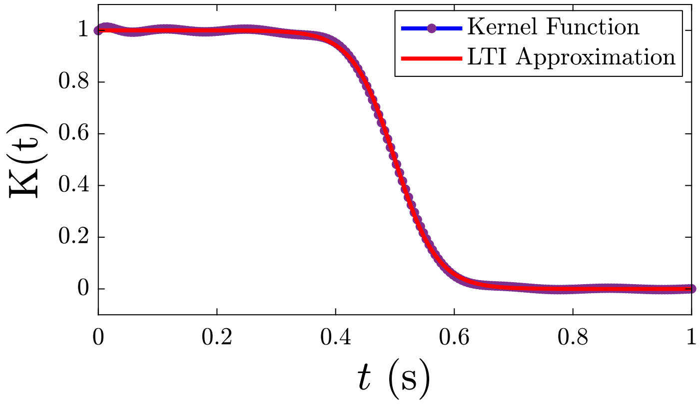

Figure 2. Kernel function $K(t) = (\tanh(-14 * (t - 0.5)) + 1)/2$ and its LTI approximation

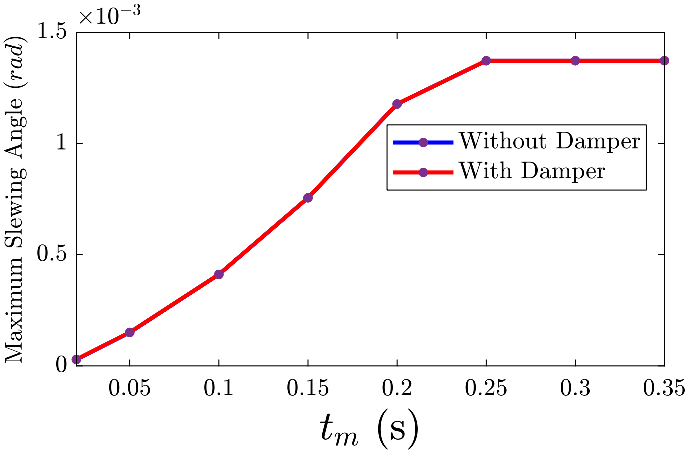

Figure 3. Comparison of maximum slewing angle with and without damper when the range of the length of panel is from 0.5 m to 2.5 m

Improvement in Maximum Slewing Angle

The chosen shape of kernel function is:

$$K(t) = \frac{\tanh(-14(t - 0.5)) + 1}{2}. \tag{18}$$

The kernel function shape and its LTI approximation is presented in Fig. 2, where t is the time scale in the material function, and $K \geq 0$ when $0 \leq t \leq 1$. This shape means that the material behaves closer to a spring, which adds more stiffness to the system at first, and closer to a damper later, which is more beneficial in the holding phase. The results are obtained using MATLAB$^{\text{TM}}$ Optimization Toolbox.

When the length of solar arrays can vary from 0.5 m to 2.5 m, the viscoelastic damper does not enhance the results. In Fig.3, two curves overlap together, and reach the upper limit of slewing capability when the slewing time is about 0.25 second. Because the optimal stiffness is inside the feasible set, the additional stiffness provided by the viscoelastic damper does not help. However, if we narrow down the range of feasible length of solar arrays to 1.5 m to 2.5 m, improvements becomes more obvious, especially when the slewing time is relatively short, as shown in Fig. 4.

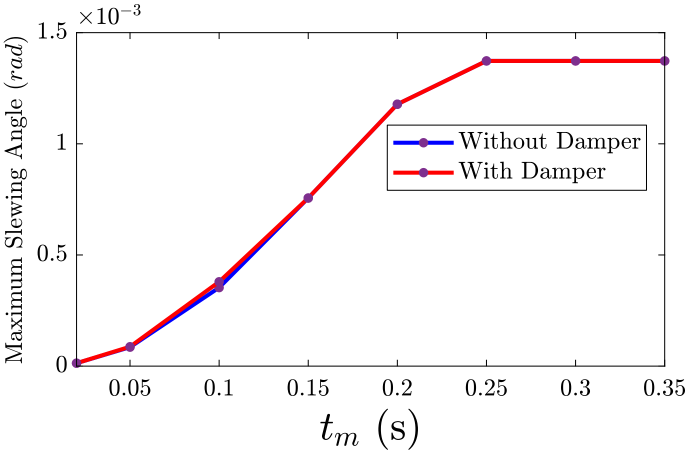

Figure 4. Comparison of maximum slewing angle with and without damper when the range of the length of panel is from 1.5 m to 2.5 m

In this case, when the slewing time is less than 0.2 second, the design with the damper shows the advantage of supplying more stiffness to the system. The maximum improvement is around 7%. As the slewing time becomes longer, the results from Fig. 3 and Fig. 4 gradually match up with each other, and they both reach the upper limit when the slewing time is longer than 0.25 second.

Improvement in Passive Damping

The viscoelastic damper also has the potential in boosting passive damping.[23] The vibration simulations are done to compare the peak vibration amplitude by disturbances with a range of different frequencies in the cases of presence and absence of the viscoelastic damper. Figure 5 and 6 are the demonstrations of the comparison.

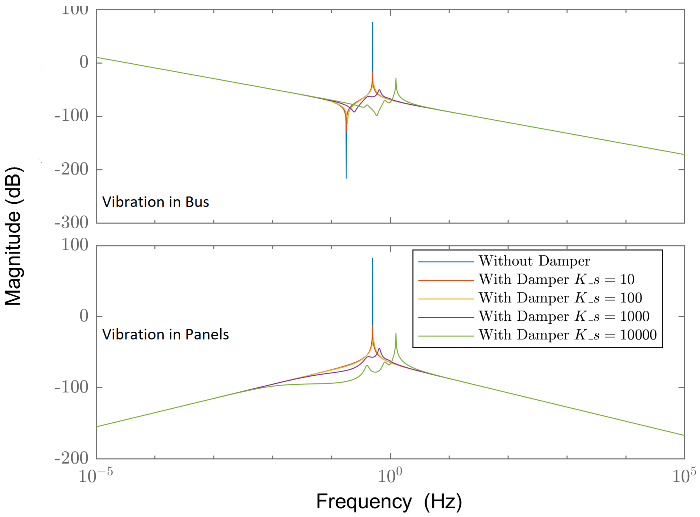

Figure 5. Passive damping comparison with different amplitudes of the kernel function, with optimal stiffness, $t_s = 1$ and K_s varied

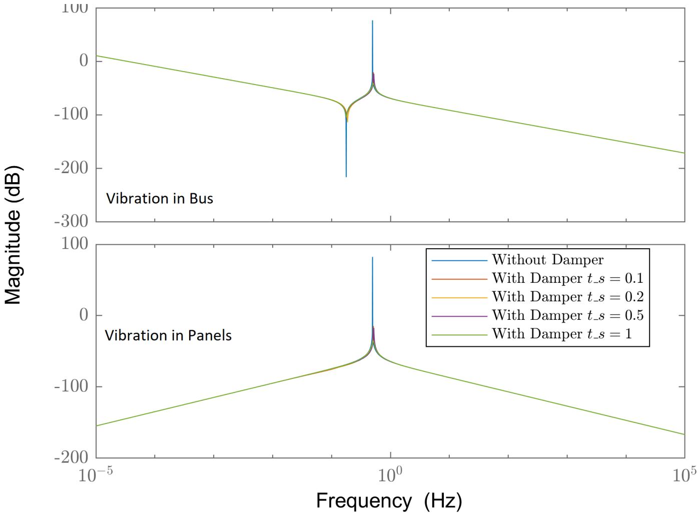

Figure 6. Passive damping comparison with different amplitudes of the kernel function, with optimal stiffness, $K_s = 100$ and t_s varied

In both figures, the top graph is the magnitude of the response of θ, and the bottom graph is the magnitude of the response of δ. The x-axis is the frequency of the disturbance in Hz. In Fig. 5, the time scale t_s is set to be 1 and K_s is varied from 10 to 10000. A large drop in magnitude and phase shifts can be observed. While in Fig. 6 , the amplitude of the kernel function is set to be 100, and t_s is varied from 0.1 to 1. With the viscoelastic damper, the peak response for both θ and δ drops significantly without any phase shifting.

This result provides another insight in design that, the properties of viscoelastic damper can provide both extra stiffness and passive damping behavior. Such properties improve the reorientation capabilities for fast pointing, and also reduce the vibrations by passive damping.

CONCLUSION

Using a case study based on a pseudo-rigid body dynamic model with a linearly viscoelastic damper, the potential benefits of viscoelastic materials within SAs are studied. Because of the characteristics of both springs and dampers, the viscoelastic material damper can provide additional stiffness to enhance the maximum slewing capability, and can reduce significantly the peak vibration induced by disturbances. Additional studies are needed, including use of higher-fidelity system models, more flexible design descriptions both for the viscoelastic material and the SAs. In particular, additional studies are needed to understand how to use distributed viscoelastic damping in a tailored manner to reduce control system complexity requirements. In addition, linking the kernel function description more closely with realizable viscoelastic materials is an important step toward realizable system designs. One possible strategy for this is to construct kernel function shape constraints based on data from existing materials. A more involved approach would be to utilize first-principles models for viscoelastic material designs.

ACKNOWLEDGMENT

This material is based upon work supported by the National Science Foundation under Grant Nos. CMMI-1463203 and CMMI-1653118.

REFERENCES

[1] A. H. de Ruiter, C. Damaren, and J. R. Forbes, Spacecraft dynamics and control: an introduction. Chichester, West Sussex: John Wiley & Sons, 1 ed., Jan. 2013.

[2] C. M. Chilan, D. R. Herber, Y. K. Nakka, S. J. Chung, F. T. Allison, J. B. Aldrich, and O. S. Alvarez-Salazar, "Co-Design of strain-actuated solar arrays for spacecraft precision pointing and jitter reduction," AIAA Journal, Vol. 55, Sept. 2017, pp. 3180–3195, 10.2514/1.J055748.

[3] S. J. C. Dyne, D. E. L. Tunbridge, and P. P. Collins, "The vibration environment on a satellite in orbit," High Accuracy Platform Control in Space, IEE Colloquium on, IET, 1993, pp. 12–1.

[4] S. Arnon and N. S. Kopeika, "Laser satellite communication network-vibration effect and possible solutions," Proceedings of the IEEE, Vol. 85, No. 10, 1997, pp. 1646–1661.

[5] A. Molter, O. A. A. da Silveira, V. Bottega, and J. S. O. Fonseca, "Integrated topology optimization and optimal control for vibration suppression in structural design," Structural and Multidisciplinary Optimization, Vol. 47, No. 3, 2013, pp. 389–397.

[6] H.-S. Yoon, "Optimal shape control of adaptive structures for performance maximization," Structural and Multidisciplinary Optimization, Vol. 48, No. 3, 2013, pp. 571–580.

[7] G. van der Veen, M. Langelaar, and F. van Keulen, "Integrated topology and controller optimization of motion systems in the frequency domain," Structural and Multidisciplinary Optimization, Vol. 51, No. 3, 2015, pp. 673–685.

[8] E. Crawley and J. de Luis, "Use of piezoelectric actuators as elements of intelligent structures," AIAA journal, Vol. 25, No. 10, 1987, pp. 1373–1385.

[9] R. E. Corman, L. G. Rao, N. A. Bharadwaj, J. T. Allison, and R. H. Ewoldt, "Setting material function design targets for linear viscoelastic materials and structures," ASME Journal of Mechanical Design, Vol. 138, Mar. 2016, p. 051402, 10.1115/1.4032698.

[10] Y. H. Lee, J. K. Schuh, R. H. Ewoldt, and J. T. Allison, "Simultaneous Design of Non-Newtonian Lubricant and Surface Texture Using Surrogate-Based Optimization," 2018 AIAA/ASCE/AHS/ASC Structures, Structural Dynamics, and Materials Conference, AIAA SciTech Forum, No. AIAA 2018-1906, Kissimmee, FL, Jan. 2018, 10.2514/6.2018-1906.

[11] R. B. Bird, R. C. Armstrong, and O. Hassager, "Dynamics of polymeric liquids. Volume 1: fluid mechanics," A Wiley-Interscience Publication, John Wiley & Sons, 1987.

[12] L. G. Rao and J. T. Allison, "Generalized viscoelastic material design with integro-differential equations and direct optimal Control," ASME 2015 International Design Engineering Technical Conferences, No. DETC2015-46768, Boston, MA, USA, Aug. 2015, pp. V02BT03A008–V02BT03A008, 10.1115/DETC2015-46768.

[13] D. R. Herber and J. T. Allison, "Unified scaling of dynamic optimization design formulations," ASME 2017 International Design Engineering Technical Conferences, No. DETC2017-67676, Cleveland, OH, USA, Aug. 2017, p. V02AT03A003, 10.1115/DETC2017-67676.

[14] Y. H. Lee, R. E. Corman, R. H. Ewoldt, and J. T. Allison, "A multiobjective adaptive surrogate modeling-based optimization (MO-ASMO) framework using efficient sampling strategies," ASME 2017 International Design Engineering Technical Conferences, No. DETC2017-67541, Cleveland, OH, USA, Aug. 2017, p. V02BT03A023, 10.1115/DETC2017-67541.

[15] L. Banjai, M. Lopez-Fernandez, and A. Schadle, "Fast and oblivious algorithms for dissipative and two-dimensional wave equations," SIAM Journal on Numerical Analysis, Vol. 55, No. 2, 2017, pp. 621–639, 10.1137/16M1070657.

[16] E. J. O. Schrama, "Three algorithms for the computation of tidal loading and their numerical accuracy," Journal of Geodesy, Vol. 78, No. 11, 2005, pp. 707–714.

[17] Z. Yu and J. Falnes, "State-space modelling of a vertical cylinder in heave," Applied Ocean Research, Vol. 17, No. 5, 1995, pp. 265–275.

[18] W. E. Cummins, "The impulse response function and ship motions," tech. rep., David Taylor Model Basin Washington DC, 1962.

[19] D. R. Herber, Advances in Combined Architecture, Plant, and Control Design. Ph.D. Dissertation, University of Illinois at Urbana-Champaign, Urbana, IL, USA, Dec. 2017.

[20] D. R. Herber, Y. H. Lee, and J. T. Allison, "DT QP Project," `https://github.com/danielrherber/dt-qp-project`, 2017.

[21] D. R. Herber and J. T. Allison, "Nested and Simultaneous Solution Strategies for General Combined Plant and Controller Design Problems," ASME 2017 International Design Engineering Technical Conferences, No. DETC2017-67668, Cleveland, OH, USA, Aug. 2017, p. V02AT03A002, 10.1115/DETC2017-67668.

[22] E. F. Crawley, “Intelligent structures for aerospace: a technology overview and assessment,” AIAA journal, Vol. 32, No. 8, 1994, pp. 1689–1699.

[23] J. L. Fanson, C.-C. Chu, B. J. Lurie, and R. S. Smith, “Damping and structural control of the JPL phase 0 testbed structure,” Journal of intelligent material systems and structures, Vol. 2, No. 3, 1991, pp. 281–300, 10.1177/1045389X9100200303.